The analysis of the calculations carried out has shown that with $\tau \leq 3$, the value of the primary extinction factor can be determined with an error of 1·5% using the following approximate expressions:

$$y_P = y_P^0(1 - 2 \tan \theta_B) + y_P^1 2 \tan \theta_B \qquad (3.2)$$

with $0 \leq \tan \theta_B \leq 0{\cdot}5$ and

$$y_P = y_P^1 = \frac{\tanh \tau}{\tau} \{1 + 0{\cdot}445 \exp[-1{\cdot}64 \tan^3 \theta_B - 1{\cdot}09(\tau - 2{\cdot}6 \cos \theta_B)^2]\}^{-1} \qquad (3.3)$$

with $0{\cdot}5 \leq \tan \theta_B \leq 1$.

In the Bragg case the primary extinction factor for the square-section parallelepiped is greater than the factor for an infinite plate of the same thickness. This difference is greatest for small Bragg angles.

Conclusions

On the basis of X-ray dynamical diffraction theory the calculations of the primary extinction factor y_P and of the profile function of the scattering curve for a crystal block in the form of a square-section parallelepiped have been carried out. The calculations made it possible to determine the character of the variation of the scattering curve as a function of the size of the crystal, the zero Fourier coefficient of polarizability and the Bragg angle. It has been found that the primary extinction factor, when the crystal size does not exceed the extinction length ($\tau \leq 1$), does not depend on Bragg angle and is determined only by the size of the crystal. When $\tau > 1$ the relationship of primary extinction factor to τ is affected by the Bragg angle. When the Bragg angle is small, the factor y_P has oscillations which are caused by the Laue diffraction contribution. Approximate relationships for estimating the primary extinction factor have been found.

References

AFANAS'EV, A. M. & KOHN, V. G. (1971). *Acta Cryst.* A**27**, 421–430.

BECKER, P. J. & COPPENS, P. (1974). *Acta Cryst.* A**30**, 129–147.

TAKAGI, S. (1962). *Acta Cryst.* **15**, 1311–1312.

TAKAGI, S. (1969). *J. Phys. Soc. Jpn*, **26**, 1239–1253.

TAUPIN, D. (1967). *Acta Cryst.* **23**, 25–28.

URAGAMI, T. (1969). *J. Phys. Soc. Jpn*, **27**, 147–154.

URAGAMI, T. (1970). *J. Phys. Soc. Jpn*, **28**, 1508–1527.

URAGAMI, T. (1971). *J. Phys. Soc. Jpn*, **31**, 1141–1161.

ZACHARIASEN, W. H. (1967). *Acta Cryst.* **23**, 558–564.

ZACHARIASEN, W. H. (1945). *X-ray Diffraction in Crystals*. New York: John Wiley.

Acta Cryst. (1978). A**34**, 326–329

Self-Crystallizing Molecular Models. V. Molecular Charge Density Contours

BY TARO KIHARA AND KAZUO SAKAI

Department of Physics, Faculty of Science, University of Tokyo, Tokyo, Japan

(*Received* 12 *September* 1977; *accepted* 26 *October* 1977)

Molecular models with magnetic multipoles, which are used for simulating crystal structures, should resemble the actual molecules not only with respect to multipoles but also in shape. To obtain better knowledge of molecular shapes, charge-density contours have been calculated and illustrated for H_2, N_2, F_2, CO_2, C_2H_2, CH_4, CF_4, BF_3 and C_2H_4. The orthorhombic, low-temperature structure of solid acetylene established by Koski & Sándor [*Acta Cryst.* (1975), B**31**, 350–353], has been discussed on the basis of the molecular shape and the mechanism of phase transition from the cubic phase.

Introduction

The molecular models with magnetic multipoles, reported in this series of papers (Kihara, 1963, 1966, 1970, 1975), were invented for the purpose of explaining the crystal structures of nonpolar molecules.

If the molecules do not possess any appreciable electric multipoles, the crystal structures are governed by the condition of closest packing of the molecules.

If, on the other hand, the molecules have sufficiently strong electric multipoles, the electrostatic interaction often governs the crystal structure. This electrostatic multipolar interaction between molecules can be replaced by magnetic interaction between molecular models with magnetic multipoles. A structure into which these models are assembled will simulate the actual crystal structure.

The molecular model should resemble the actual

molecule not only with respect to the multipole but also in shape. It is true that, in some respect, the shape of a molecule may be simplified, or idealized, in its model; the molecule of benzene, for example, is represented by an axially symmetric model. However, an oblate spheroidal model cannot be used for benzene. Similarly, the molecule of cyanogen N≡C–C≡N cannot be represented by a model of convex shape.

In parts II and IV, a prolate spheroidal quadrupolar model was introduced for acetylene HC≡CH. Part IV contains the following statement: 'A cubic *Pa*3 structure with four molecules per unit cell and an orthorhombic *Pnnm* structure with two molecules per unit cell are formed by this model. The former simulates the crystal structure of acetylene above −140°C; the latter simulates, probably, the unestablished structure below −140°C.'

The low-temperature modification of solid acetylene, however, has been established by Koski & Sándor (1975) to be *Cmca* with four molecules per unit cell, by neutron powder diffraction study of C_2D_2. Thus it has been revealed that a prolate spheroid does not correctly represent the shape of the molecule of acetylene.

Better knowledge of the shape of molecules is now needed. The present paper starts from a correct understanding of the molecular shape – the shape of the electron cloud in a molecule.

Charge-density contours

The contours of charge density in atomic units are illustrated in Figs. 1–9 for typical nonpolar molecules. '1 A.U.' means the unit length in atomic units, or the Bohr radius, 0·529 Å. The outermost contour indicates a charge density 0·002, or 0·002 e per cubic Bohr radius. It has been confirmed that this contour represents the size and shape of the molecule in gaseous and solid states. The density value of the nth contour from the outermost is $0{\cdot}002 \times 2^{n-1}$.

For CH_4 and for CF_4, the charge-density distribution is shown by a set of density contours in a plane of symmetry; for BF_3 and for C_2H_4, in two orthogonal planes of symmetry.

All these contours have been calculated on the basis of Snyder & Basch's (1972) table of molecular wave

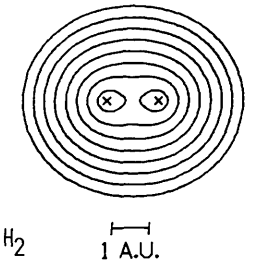

Fig. 1. Electron-density distribution in hydrogen. The density value of the nth contour from the outermost is $0{\cdot}002 \times 2^{n-1}$ in atomic units.

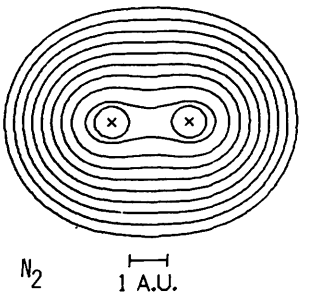

Fig. 2. Electron-density distribution in nitrogen.

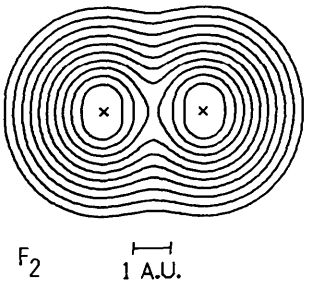

Fig. 3. Electron-density distribution in fluorine.

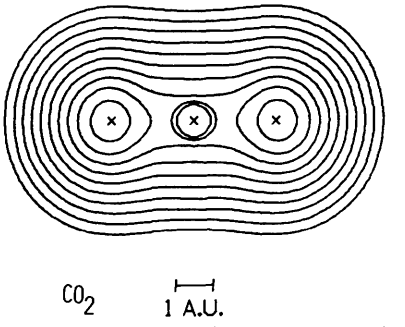

Fig. 4. Electron-density distribution in carbon dioxide.

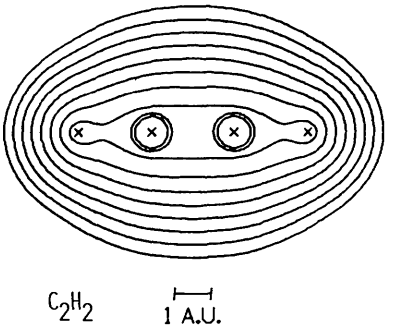

Fig. 5. Electron-density distribution in acetylene.

functions, which are composed of Gaussian rather than exponential functions. The use of a set of Gaussian functions, however, does not affect the results as long as the density is larger than 10^{-3} in atomic units. The charge-density contours for N_2, F_2 and CH_4 are consistent with the results of other authors (Bader, Hennecker & Cade, 1967; Turner, Saturno, Hauk & Parr, 1963).

For H_2, N_2, CO_2 and CF_4, these figures consolidate the foundation of our molecular models (Models 1, 2 and 11 in part IV).

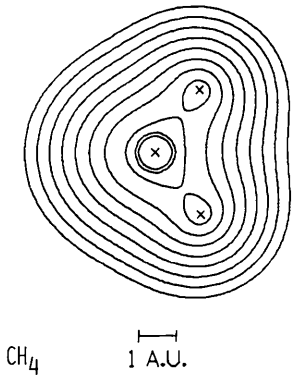

Fig. 6. Electron-density distribution in methane.

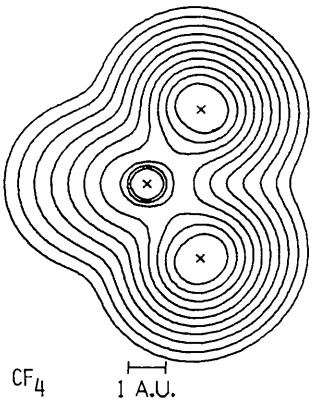

Fig. 7. Electron-density distribution in carbon tetrafluoride.

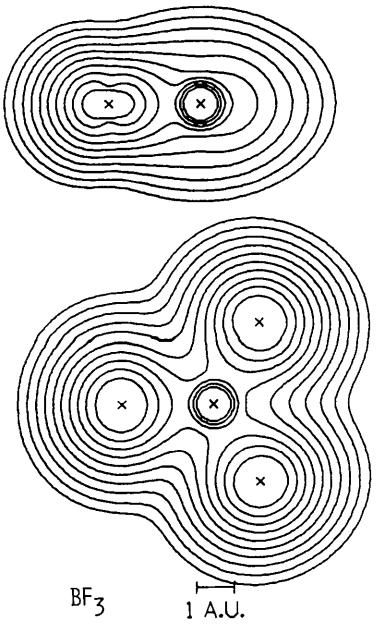

Fig. 8. Electron-density distribution in boron trifluoride.

Phase transition in solid acetylene

On the basis of Fig. 5, the molecular model of acetylene should be as in Fig. 10. By this model the othorhombic *Cmca* and *Pnnm* structures can be formed as well as the cubic *Pa*3 structure. It is not possible, therefore, to explain the reality of *Cmca* by means of our molecular model alone.

The following is, however, a satisfactory explanation. Since the thermal motions result in the enlargement of the effective size of molecules, the molecular shape at high temperatures is effectively closer to a sphere

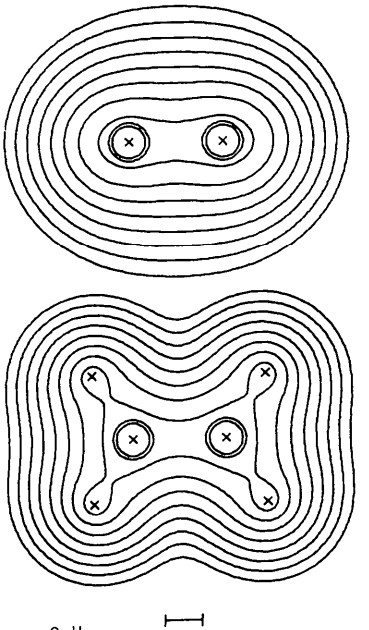

Fig. 9. Electron-density distribution in ethylene.

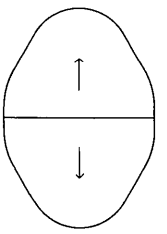

Fig. 10. Magnetic model of the acetylene molecule.

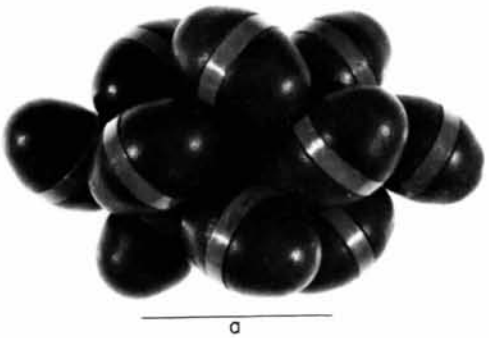

Fig. 11. Cubic *Pa*3 structure simulating the crystal structure of acetylene at high temperatures.

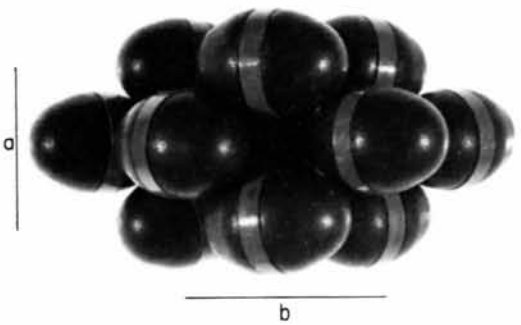

Fig. 12. Orthorhombic *Cmca* structure simulating the crystal structure of acetylene at low temperatures.

than at low temperatures. The high-temperature structure of solid acetylene is in fact cubic *Pa*3, the characteristic structure into which quadrupolar spheres are assembled. This cubic structure (Fig. 11) can change to *Cmca* (Fig. 12) by rotation of the molecules through an angle 45°, whereas the rotation of some molecules through 90° is necessary for the transition to *Pnnm* (compare Fig. 11 and Fig. 12 in part II). The barrier to *Cmca* is possibly lower, thus favouring the transition to this structure.

A unit cell of the *Cmca* structure in which our molecular models are assembled has the ratios $a/c = 0{\cdot}85$ and $b/c = 0{\cdot}95$, which correspond to $a/c = 0{\cdot}896$ and $b/c = 0{\cdot}970$ observed by Koski & Sándor (1975).

One of the authors (TK) thanks Dr H. K. Koski for useful information. Thanks are due to Dr K. Miyoshi for valuable advice on the display of charge-density contours.

References

BADER, R. F. W., HENNEKER, W. H. & CADE, P. E. (1967). *J. Chem. Phys.* **46**, 3341–3363.
KIHARA, T. (1963). *Acta Cryst.* **16**, 1119–1123.
KIHARA, T. (1966). *Acta Cryst.* **21**, 877–879.
KIHARA, T. (1970). *Acta Cryst.* A**26**, 315–320.
KIHARA, T. (1975). *Acta Cryst.* A**31**, 718–721.
KOSKI, H. K. & SÁNDOR, E. (1975). *Acta Cryst.* B**31**, 350–353.
SNYDER, L. C. & BASCH, H. (1972). *Molecular Wave Functions and Properties*. New York: John Wiley.
TURNER, A. G., SATURNO, A. F., HAUK, P. & PARR, R. G. (1963). *J. Chem. Phys.* **40**, 1919–1928.

Acta Cryst. (1978). A**34**, 329–336

Elimination of Extinction by a Temperature Gradient

BY PAUL SEILER AND JACK D. DUNITZ

Organic Chemistry Laboratory, Swiss Federal Institute of Technology, ETH-Zentrum, 8092 *Zürich, Switzerland*

(*Received* 7 *October* 1977; *accepted* 5 *November* 1977)

Experiments with crystals of a $KNCS.C_{12}H_{24}O_6$ complex show that the integrated intensities of reflections showing strong extinction can be raised to their expected kinematic values when the crystal is subjected to a temperature gradient. The intensity increases are accompanied by a broadening of the diffraction peaks and are reversible with no detectable hysteresis. These observations seem to be incompatible with the mosaic-crystal model. Local variations in the extinction behaviour have been detected by using a fine incident beam and suggest inhomogeneity of crystal texture. The intensity increases are probably connected with a reduction in the mean size of the perfect crystal domains, *i.e.* with a decrease of the mean spatial correlation length within the crystal.

Introduction

Extinction is one of the most serious problems in accurate X-ray diffraction intensity measurements. The present paper describes some experiments that bear on this problem. It is shown that application of a temperature gradient (TG) to a crystal during the diffraction process can reduce, or in some cases even eliminate,